Arabian Journal for Science and Engineering
https://doi.org/10.1007/s13369-018-3543-1

RESEARCH ARTICLE - PHYSICS

# Study of Structural, Magnetic and Optical Properties of $BiFeO_3-PbTiO_3$ Multiferroic Composites

**Mohammad Shariq[1] · Davinder Kaur[2] · Vishal Singh Chandel[3] · Praveen K. Jain[4] · Sasi Florence[1] · Mukul Sharma[5] · Shahir Hussain[6]**

Received: 14 May 2018 / Accepted: 29 August 2018


**Abstract**
The crystalline samples of lead titanate altered bismuth ferrite $(BiFeO_3)_{1-x}(PbTiO_3)_x$ [$x = 0, 0.1, 0.2, 0.3, 0.4$ and 0.5] have been synthesized by high-temperature solid-state reaction technique. The formation of the materials was affirmed through fundamental investigation utilizing X-ray diffraction which uncovers the presence of morphotropic phase boundary (MPB) in composite. XRD examination displays structural change from rhombohedral ($x = 0.0$) to tetragonal ($x = 0.4$). Estimated grain size along (104) peak was observed to be diminished with the increase in content of $PbTiO_3$ due to mixing of tetragonal phases. SEM and EDAX of sample were carried out for analysis of surface morphology and verification of chemical homogeneity, respectively. Study of M-H graph reveals antiferromagnetic nature of $BiFeO_3$. Magnetic measurement of $(BiFeO_3)_{1-x}(PbTiO_3)_x$ ceramics shows weak-induced ferromagnetism by substituent effects at temperature of 5 K. Low-temperature magnetic measurement under ZFC reveals an anomaly in tetragonal phase of MPB for composition $x = 0.2$ and 0.3. With respect to $BiFeO_3$, $BiFeO_3-PbTiO_3$ ceramics displays advancement in the electric polarization. Direct and indirect band gaps are modified with variation of $PbTiO_3$ in $BiFeO_3-PbTiO_3$ composites.

**Keywords** $(BiFeO_3)_{1-x}(PbTiO_3)_x$ ceramics · Antiferromagnetic · Multiferroic · SQUID

## 1 Introduction

Multiferroics materials that couple order parameter such as electric, magnetic and structural appearing the concurrence of ferroelectric, ferromagnetic and ferroelastic behaviors have attracted recently in the fabrication of multifunctional devices [1]. The great interest in this class of solids is due to their innovative potential applications. Controlling magnetization utilizing external electric field or vice versa brought the way of new multifunctional devices, such as novel data memory, spintronics devices and new kinds of sensors [2,3].

$BiFeO_3$ (BFO) received great attention among the known multiferroic materials, as prime candidate for room-temperature application due to high temperature of ferroelectric and antiferromagnetic ordering [4]. $BiFeO_3$ has many interesting characteristics including high ferroelectric Curie (1043 K), high magnetic Neel temperatures (647 K), large characteristics polarization 100 $\mu s/cm^2$ along [111] direction and high magnetoelectric coupling coefficient [5,6]. Morphotropic phase boundary (MPB) of high piezoelectric coefficient makes BFO valuable for several devices [7]. Because of high unconstrained polarization (Ps), observed in the BFO thin films [8,9], it is appropriate for high memory gadgets. But inverse to this, bulk BFO has low polarizations [10].

In spite of the different points of interest, unfortunately, the BFO material has some intuitive issues, for example development of secondary phases, absence of structural dis-

✉ Mohammad Shariq
aligshariq@gmail.com; mohammadshariq@jazanu.edu.sa

1 Department of Physics, Faculty of science, Jazan University, Jazan, Saudi Arabia

2 Functional Nanomaterials Research Laboratory, Department of Physics and Centre of Nanotechnology, Indian Institute of Technology, Roorkee 247667, India

3 Department of Applied Science and Humanities, Rajkiye Engineering College, Ambedkar Nagar, UP, India

4 Swami Keshvanand Institute of Technology, Management and Gramothan, Jaipur, India

5 Centre for Environmental Research and Studies, Jazan University, Jazan, Saudi Arabia

6 Department of Electrical Engineering, Jazan University, Jazan, Saudi Arabia

Published online: 07 September 2018

tortion, spiral spin modulation, weak magnetoelectric effect and presence of leakage current. The thermodynamically stable impurity phases such as $Bi_2Fe_2O_9$ and $Bi_{25}FeO_{40}$ are formed along with $BiFeO_3$ phase [11,12]. As a result of high electrical conductivity of the material, the material is not exceptionally appropriate for some applications. There is absence of homogeneous antiferromagnetic spin order of $BiFeO_3$ instead; disproportionately, modulated spin structure is available, which appears as incommensurate cycloid with long wavelength $\lambda$ of $\sim$ 600 Å [13]. Appearance of cycloid spins arrangement destroys the macroscopic magnetization emerging from Dzyaloshinskii–Moriya (D-M) interaction and restrains the direct magnetoelectric impact [14]. The spiral spin in $BiFeO_3$ is independent on the applied magnetic field and temperature, but substituent effect can break translational symmetry of the spiral spin modulation in BFO or other perovskites [15,16]. Impurity-free $BiFeO_3$ has large polarization and high resistivity, but it is not easy to keep $Bi_2O_3$ and $Fe_2O_3$ in stoichiometry during high-temperature synthesis of BFO due to volatile nature of $Bi_2O_3$, giving impurity of $Bi_2Fe_4O_9$. The formation of $Bi_2Fe_4O_9$ can be avoided by adding some extra amount of $Bi_2O_3$, but simultaneously it introduces creation of another Bi-rich $Bi_{25}FeO_{40}$ secondary phase. These problems can be removed by fast thermal process with a high warming rate around 50 °C/s to limit the vanishing of $Bi_2O_3$ during the synthesis process of the $BiFeO_3$, [4,17] and quenching process was introduced to solidify the metastable $BiFeO_3$ [10]. In order to improve multiferroic properties of BFO, substitution of different rare earths or other reasonable ions, for example $Nd^{3+}$, $La^{3+}$, $Ba^{2+}$ and $Sm^{3+}$ at the Bi site, whereas $Ti^{4+}$, $Mn^{4+}$, $Co^{3+}$ and $Nb^{5+}$ are delegated at the Fe site [18–21]. The synthesis of composite with different materials and the substitution of other impurity atoms are assumed to curb the firmness of the perovskite structure and the vaporous behavior of Bi ions and to reduce the formation of oxygen vacancies for charge compensation. In recent years, numerous literary works have mentioned that proper $BiFeO_3$ phases are stabilized by the formation of composite with $PbTiO_3$ or $BaTiO_3$ and different properties have been greatly improved [4,22–24]. Recently, N. panda and his co-worker reported enhanced dielectric constant of $BiFeO_3-PbTiO_3$ and strong correlation between the microstructural and impedance parameters [5]. Pradhan et al. [23] studied La-modified $(BiFeO_3)_{1-x}(PbTiO_3)_x$ system and observed multiferroic properties which are evident from measurement of ferroelectric loops and magnetoelectric coefficient. In our previous recent work, we studied structural, magnetic and optical properties of binary multiferroic $(BiFeO_3)_{1-x}(BaTiO_3)_x$ and observed great improvement in multiferroic properties of composite [4]. Introduction of lead titanate ($PbTiO_3$) in the present work settles the perovskite phase of composite as well as creates a MPB with $BiFeO_3$ because of the distinction in crystal symmetry between $PbTiO_3$ and $BiFeO_3$. So, the BF–PT composite can be viewed as an option among piezoelectric and ferroelectric materials that can be utilized as a part of innovative applications [25]. The present study focused on the synthesis of $(BiFeO_3)_{1-x}(PbTiO_3)_x$ [BF–PT] composite and investigation of structural, magnetic and optical properties of BF–PT. It would be of considerable difference to investigate direct and indirect energy band of various compositions of $(BiFeO_3)_{1-x}(PbTiO_3)_x$ composite as it is not found in previous studies.

## 2 Experimental Work

Taking $BiFeO_3$ and $PbTiO_3$ separately in stoichiometric extents, crystalline $BiFeO_3-PbTiO_3$ solid solution was prepared by solid-state reaction process. First of all, $PbTiO_3$ was synthesized by using high-purity oxides of PbO and $TiO_2$ as reactants followed by calcinations at 800 °C for 2 h. Calcinated powder was sintered in furnace at temperature of 900 °C to get the phase formation of $PbTiO_3$. In similar way, $BiFeO_3$ ceramics was set up from $Bi_2O_3$ and $Fe_2O_3$ as reactants by solid-state reaction method followed by calcination at the 600 °C for 2 h and sintering at temperature of 870 °C for 300 seconds. To stay away from secondary phase of $Bi_2Fe_4O_9$ and $Bi_2O_3$ during synthesis process, 10% surplus amount of $Bi_2O_3$ was supplemented to the beginning reactants.

Various compositions of $(BiFeO_3)_{1-x}(PbTiO_3)_x$ composite were synthesized by taking content of $PbTiO_3$ from 10% to 50%. $BiFeO_3$ and $PbTiO_3$ were taken separately in stoichiometric sums and crushed in agate mortar through dry mode for 4 h and then followed by wet granulating for 2 h utilizing methanol. Samples were calcinated at temperature of 800 °C for 2 h. All samples of composite were mixed with a couple of drops of 5 % concentrated fluid polyvinyl alcohol (PVA) binder and again grinded in the agate mortar for 2 h. Blended powders with various compositions were squeezed into circular disks with a pressure of $1.5 \times 10^8$ Pascal. These disk-shaped pellets of various compositions were warmed at 260 °C for 1 h to evaporate PVA binder. The pellet samples kept with open alumina crucible were sintered at 950 °C for 2 h. The samples are assigned name according to their compositions; for example, 90BF-10PT refers to $(BiFeO_3)_{0.9}(PbTiO_3)_{0.1}$ and so on.

The phase formation and structural information of sample materials were examined by an XRD data utilizing Bruker AXS D-8 advanced diffractometer. The XRD pattern of samples was recorded at normal temperature with Cu Kα radiation (1.54 Å) and step size of 0.02°. Scanning electron microscopy was utilized for study of surface morphology of composite. Atomic and weight percentages of individual elements Bi, Fe, O, Pb and Ti in the sample material were

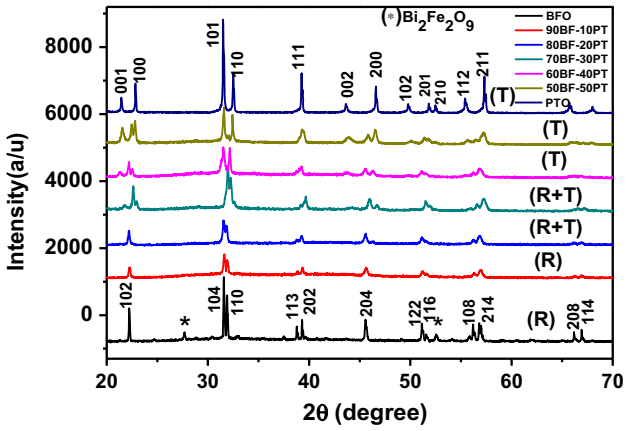


**Fig. 1** XRD patterns of $(BiFeO_3)_{1-x}(PbTiO_3)_x$ solid solution along with $BiFeO_3$ and $PbTiO_3$

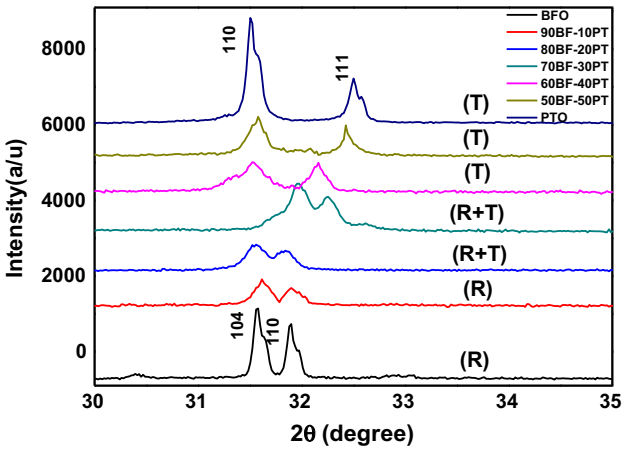


**Fig. 2** XRD profiles of $(BiFeO_3)_{1-x}(PbTiO_3)_x$ solid solution with the MPB along with peak (104), (110) of $BiFeO_3$ and (110), (111) of $PbTiO_3$

confirmed by energy-dispersive X-ray analysis (EDAX). The sintered pellets of different samples were electroded using high conducting silver paste for the measuring electrical parameters. Polarization versus electric field (P-E) hysteresis loops of $(BiFeO_3)_{1-x}(PbTiO_3)_x$ were measured by utilizing precision premier II (Radiant technology) ferroelectric tester. Magnetic properties were investigated by super conducting quantum interference device (SQUID, Quantum Design MPMS XL) magnetometer. A UV–Vis–NIR spectrometer (Varian Cary 5000 model) was utilized in measurement and calculation of different optical constants of BF–PT composites.

## 3 Results and Discussion

Figure 1 shows XRD patterns of the sintered pellets of BF–PT ceramics. X-ray diffraction peaks of all samples were recorded utilizing standard PC software PCPDFWIN [26]. The solid solution BF–PT was crystallized in the perovskite phase, without forming Bi-rich secondary phases like $Bi_2Fe_4O_9$, $Bi_{25}FeO_{40}$, whereas $BiFeO_3$ ceramics was solidified in the perovskite phase with a little amount of $Bi_2Fe_4O_9$ phase. With the content of $PbTiO_3$, rhombohedral phase is changed into mixture of morphotropic phases, and afterward, tetragonal phase is confirmed. Figure 2 demonstrates the presence of rhombohedral and tetragonal in morphotropic phase boundary region. It has extraordinary significance in light of the fact that MPB should be the key behind the extensive piezoelectric coefficients of PZT [27,28], so MPB of BF–PT may drag substantial piezoelectric constants.

Room-temperature lattice constants of BF–PT system with different compositions were calculated by formulae

$$\frac{1}{d_{hkl}^2} = \frac{\left(h^2+k^2+l^2\right)\sin^2\alpha + 2\left(hk+kh+hl\right)\left(\cos^2\alpha-\cos\alpha\right)}{a^2\left(1-3\cos^2\alpha+2\cos^3\alpha\right)} \quad \text{(Rhombohedral phase)} \tag{1}$$

$$\frac{1}{d_{hkl}^2} = \frac{h^2+k^2}{a^2} + \frac{l^2}{c^2} \quad \text{(Tetragonal phase)} \tag{2}$$

and are shown in Table 1 where $d_{hkl}$ is interplanar distance, $h, k, l$ are Miller indices of the Bragg plane and $\alpha$ is internal angle. These calculated lattice parameters are near to those effectively revealed for polycrystalline $BiFeO_3-PbTiO_3$ [34].

Amended form of Scherrer formula can be used for calculation of crystallite size ($D_{hkl}$) of the recognized crystalline phase

$$D_{hkl} = \frac{k\lambda}{\beta\cos\theta} \tag{3}$$

$D_{hkl}$ is average crystalline size, $K$ is a dimension free shape factor which has value close to unity (0.9), λ is wave length of X-ray belonging to Cu $K_{\alpha 1}$, $\beta$ is the line broadening (FWHM) excluding line broadening due to instrument, and $\theta$ is the Bragg angle. The grain size was assessed along (104) peak and observed to be diminished with increment in content of $PbTiO_3$ due to mingling of tetragonal phases. In the rhombohedral phase, lattice constant 'a' increased, while in the case of tetragonal phase lattice parameters 'a' increased and 'c' decreased. So, it could be presumed that lattice constants of the $(BiFeO_3)_{1-x}(PbTiO_3)_x$ system were not increased monotonically with increasing '$x$,' but it showed fluctuation. The radius of $Bi^{+3}$ is smaller than that of $Pb^{+2}$, while the radius of $Fe^{+3}$ is larger than that of $Ti^{+4}$. In this way, substitution of Pb on Bi site will come about an increase in lattice parameter, while it is the opposite for the Ti substitution at location of Fe. So, introduction of $PbTiO_3$ is responsible for the variance of lattice parameter. The lattice parameters of rhombohedral and tetragonal phases were

**Table 1** Various parameters of $(BiFeO_3)_{1-x}(PbTiO_3)_x$ with different compositions

| Composition $x$ | Phase structure | $2\theta$ (°) | FWHM (°) | $D_{hkl}$ Par. size (nm) | Lattice parameter (Å) | c/a ratio | Volume of unit cell (Å$^3$) |
|---|---|---|---|---|---|---|---|
| 0 | Rhombohedral | 31.56 | 0.141 | 66.5 | $a_r = 5.623$<br>$\alpha = 59.38$ | 1 | 123.941 |
| 0.1 | Rhombohedral | 31.61 | 0.192 | 49.1 | $a_r = 5.636$<br>$\alpha = 59.45$ | 1 | 125.005 |
| 0.2 | Rhombohedral and tetragonal | 31.55 | 0.231 | 40.6 | MPB | – | |
| 0.3 | Rhombohedral and tetragonal | 31.95 | 0.252 | 37.4 | MPB | – | |
| 0.4 | Tetragonal | 31.53 | 0.293 | 32.1 | $a_t = 3.851$<br>$c_t = 4.431$ | 1.150 | 65.712 |
| 0.5 | Tetragonal | 31.58 | 0.431 | 20.2 | $a_t = 3.860$<br>$c_t = 4.353$ | 1.127 | 64.857 |
| 1.0 | Tetragonal | 31.50 | 0.151 | 63.1 | $a_t = 3.898$<br>$c_t = 4.310$ | 1.105 | 65.480 |

calculated based on R3m & P4mm symmetry, respectively. Volume of unit cells for rhombohedral and tetragonal phase of $(BiFeO_3)_{1-x}(PbTiO_3)_x$ at various values of '$x$' is given in Table 1. Increasing Pb content prompts slight increment in volume of rhombohedral unit cell. This change is primarily because of the bigger ionic radii of Pb (1.37 A°) in comparison with ionic radii of Bi (1.19 A°). The volume of tetragonal unit cell decreases slightly with $x$ then increased for $x = 1$.

Figure 3 demonstrates SEM micrograph of $(BiFeO_3)_{0.9}(PbTiO_3)_{0.1}$ sintered at 950 °C, which showed almost uniform grain size and dissemination. It uncovered the average grain size of ceramics 90BF-10PT approximately 1–2 μm. Overall particle estimate appeared by FE-SEM was much bigger in comparison with particle size estimated from the XRD outcome (Table 1). This was because of fact that XRD calculation provides the normal mean crystallite estimate, while FE-SEM indicates agglomeration of the particles. The XRD and FE-SEM data can be obliged by the way that smaller primary particles have a broad surface free energy, so these smaller particle would tend to agglomerate quickly and grow into bigger grains. EDAX in Fig. 4 shows the atomic and weight percentage of individual components present in 90BF-10PT sample. The atomic and weight percentages of elements obtained by EDAX in the ceramics sample 90BF-10PT are much near to their genuine esteems.

In Fig. 5, linear change of magnetization of $BiFeO_3$ versus magnetic field at room temperature confirms antiferromagnetic nature of BFO as reported in other studies [4,12]. Net magnetic moment from canted antiferromagnetic spins is spacially resulted to zero because of cycloidal rotation of resultant spins, explaining antiferromagnetic nature of BFO [29]. Figure 6 shows the variation of magnetization (M) with magnetic field of ceramics $(BiFeO_3)_{1-x}(PbTiO_3)_x$ at 5 K.

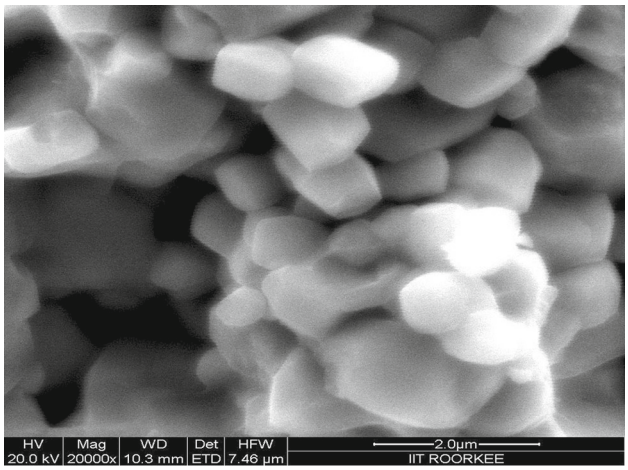


**Fig. 3** SEM image of $(BiFeO_3)_{0.9}(PbTiO_3)_{0.1}$ solid solution sintered at 950 °C

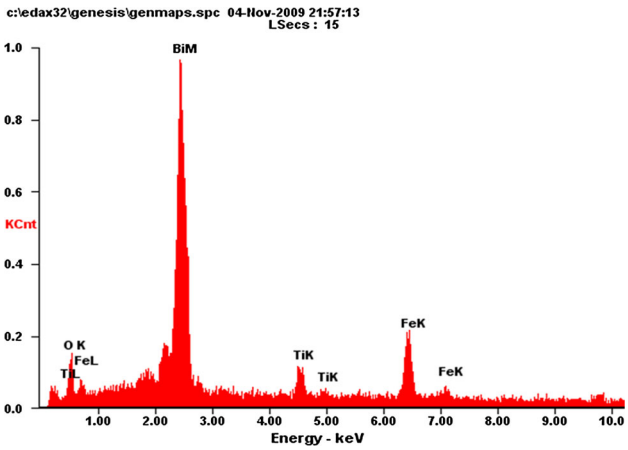


**Fig. 4** EDAX spectrum of ceramics sample $(BiFeO_3)_{0.9}(PbTiO_3)_{0.1}$

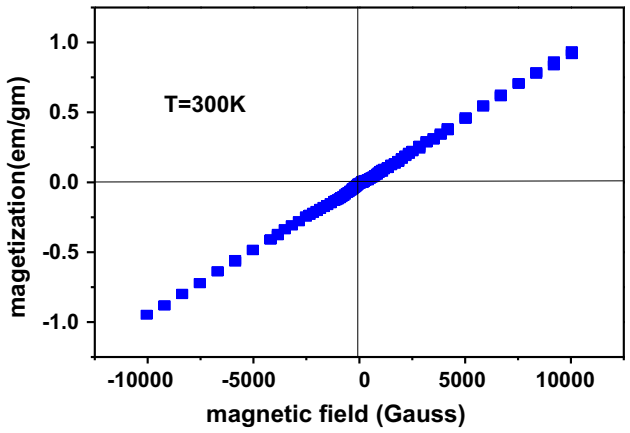


**Fig. 5** Magnetization (M) versus applied magnetic field (H) for $BiFeO_3$ at temperature of 300 K

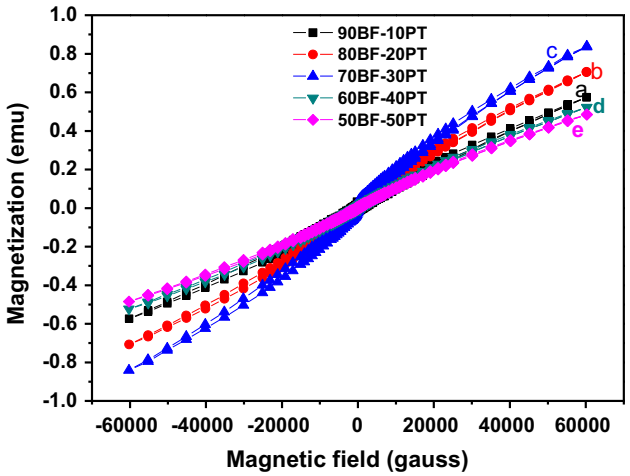


**Fig. 6** Magnetization (M) as function of magnetic field (H) for $(BiFeO_3)_{1-x}(PbTiO_3)_x$ at 5 K with different compositions (a) $x = 0.1$, (b) $x = 0.2$, (c) $x = 0.3$, (d) $x = 0.4$ and (e) $x = 0.5$

Weak ferromagnetism was observed in BF–PT system by the substitution effect of $PbTiO_3$. Ferromagnetism in BF-BT may rely on structural distortion to destroy the inhomogeneous spin structure with regard to spin cycloid of BFO correlative to its *R*3*c* structure [30]. Then again, the distributions of $Ti^{4+}$ and $Fe^{3+}$ ions in the octahedral positions additionally influence the magnetization in composite. So, there is equivalent possibility that both the structural distortion and the $Fe^{3+}$ ion distribution can play significant role in the commencement of ferromagnetism and in magnetic properties of BF–PT system [31]. Table 2 shows the remnant magnetization and coercivity of ceramics BF–PT with relatively strong magnetization $31.41 \times 10^{-3}$ emu/gm and incredible decrease in coercive magnetic field 510.22 Gauss for composition of 70BF-30PT. High relative estimation of magnetization at $x = 0.3$ might be ascribed to the occupancy of $Ti^{4+}$ in the B position, which prompts to the abolition of canting spin structure and gives extensive magnetization. Reduction in remnant magnetization for $x \geq 0.4$ might be ascribed to noteworthy substitution of $Ti^{3+}$ in B site that reduces total $\mu_B$ in unit volume. So, $Ti^{3+}$ substitution in B site weakens the improved magnetization from abolition of canting of spin structure and so reduces the magnetization.

In Fig. 7, low-temperature (5–300 K) magnetization of $(BiFeO_3)_{1-x}(PbTiO_3)_x$ ceramics samples was measured in the external field of 1kOe under zero-field cooling (ZFC) condition. Steep rise in magnetization was observed at lower value of temperature for all compositions. This is standard behavior for ferromagnetic materials and can be assumed as a result of the decrement in thermal energy [32]. Maximum magnetization was observed in $(BiFeO_3)_{0.7}(PbTiO_3)_{0.3}$ sample at all temperature, in concurrence with optimum magnetization acquired for this composition in M-H plot (Fig. 6). Change of magnetization versus temperature for different values of '*x*' may depend on various factors, for example (i) structural distortion because of Pb, Ti replacement, (ii) reduced particle size, (iii) change in the oxygen stoichiometry and (iv) variation of magnetic anisotropy. Paramagnetic–antiferromagnetic phase transition of rhombohedral $BiFeO_3$ ($T_{N-r} = 600$ K) is reported in Refs. [33]. Zhu *et al.* [34] reported that different phases in MPB composition undergo an antiferromagnetic ordering at particular temperature, showing to an anomaly in graph of magnetization versus temperature (M-T). The ZFC magnetization measurement of $0.67BiFeO_3-0.33PbTiO_3$ crystal from 2 to 600 K is reported in another research article of Zhu et el. [35]. Due to unavailability of oven attachment in SQUID, we performed only low-temperature (5–300 K) magnetic moment measurement under ZFC (Fig. 7). We observed an anomaly in tetragonal phase of MPB for composition $x = 0.2$ and 0.3 as visible seen in inset of Fig. 7. Antiferromagnetic transition temperature ($T_{N-t}$) corresponding to tetragonal phase for $x = 0.2$ and 0.3 was measured as 252 K and 243 K, respectively. So we concluded that in the MPB from $x = 0.2$ to 0.3, antiferromagnetic transition temperature ($T_{N-t}$) corresponding to tetragonal phase decreased with the increase in '*x*'. Our outcome estimation of $T_{N-t}$ for $x = 0.2$ and 0.3 is different, as $T_{N-t}$ reported by Zhu et el. [34] 260 K, 251 K corresponding to $x = 0.2$ and $x = 0.28$.

Figure 8 demonstrates the ferroelectric hysteresis loops (P-E) of $(BiFeO_3)_{1-x}(PbTiO_3)_x$ at 1 Hz frequency with electric field of 40 kV/cm. Weak polarization 0.07 $\mu C/cm^2$ was seen for $BiFeO_3$ under an electric field of 40 kV/cm. It recommends exceedingly conductive nature of BFO at room temperature and only fractional inversion of the polarization occurs, which is credited to the changeable oxidation states of Fe ions (from $Fe^{+2}$ to $Fe^{+3}$). It also reported by Das and his co-workers that high leakage characteristics of BFO ceramics could produce difficulty in attaining saturated polarization [36]. Because of moderately huge leak-

**Table 2** Optical band gap, remnant magnetization and coercivity of BFO and BF–PT composites

| Composition ($x$) | Direct band gap (eV) | Indirect band gap (eV) | Remnant magnetization (emu/gm) $10^{-3}$ | Coercivity (Gauss) |
|---|---|---|---|---|
| 0.00 | 2.49 | 1.71 | 24.05 | 1968.19 |
| 0.10 | 2.58 | 1.89 | 18.23 | 1147.40 |
| 0.20 | 2.62 | 1.97 | 31.41 | 510.22 |
| 0.30 | 2.78 | 2.03 | 13.82 | 614.09 |
| 0.40 | 2.84 | 2.10 | 07.23 | 645.76 |

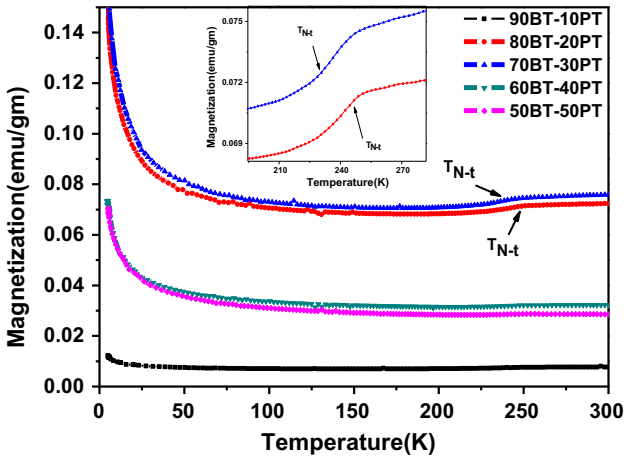


**Fig. 7** Variation of magnetization with temperature of $(BiFeO_3)_{1-x}(PbTiO_3)_x$ system for composition of $x = 0.1, 0.2, 0.3, 0.4$ and 0.5

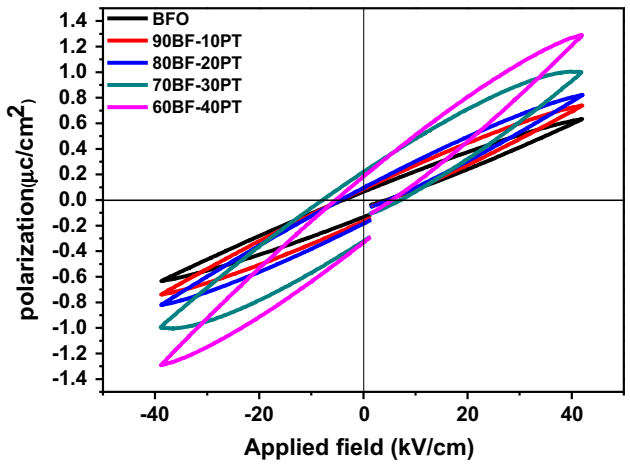


**Fig. 8** Polarization versus electric field curves of $(BiFeO_3)_{1-x}(PbTiO_3)_x$ at room temperature with composition $x = 0, 0.1, 0.2, 0.3$ and 0.4

age current, just low field hysteresis loops were acquired for $(BiFeO_3)_{1-x}(PbTiO_3)_x$ ceramics. Content of $PbTiO_3$ in BF–PT system upgraded the sintering ability and decreased oxygen vacancies. Consequently, remnant polarization was increased, but the hysteresis loop could not be saturated up to $x = 0.2$. P-E hysteresis loops of $(BiFeO_3)_{1-x}(PbTiO_3)_x$

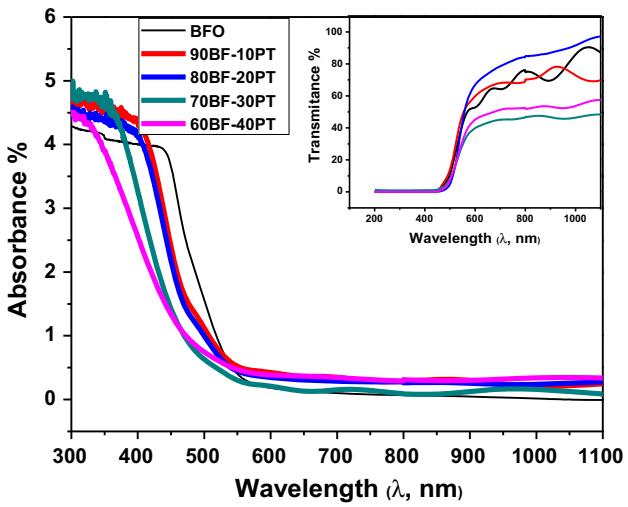


**Fig. 9** Absorbance spectra of $(BiFeO_3)_{1-x}(PbTiO_3)_x$ composites. Inset shows transmittance % of $(BiFeO_3)_{1-x}(PbTiO_3)_x$ composite with composition $x$

ceramics at 30% mol and 40% mol of $PbTiO_3$ were achieved toward the saturation due to stabilization of the perovskite structure and decline in $Fe^{+2}$ ions and oxygen vacancies, trailed by volatilization of Bi or Pb [37].

Absorption spectra of $(BiFeO_3)_{1-x}(PbTiO_3)_x$ ceramics were recorded as a function of wavelength of range 300–1100 nm (Fig. 9). Inset of Fig. 9 demonstrates the optical transmission spectra of $(BiFeO_3)_{1-x}(PbTiO_3)_x$ composites. At the wavelength of 500–540 nm, the transmission of BFO and its composite $(BiFeO_3)_{1-x}(PbTiO_3)_x$ diminishes rapidly and finally reaches to zero at around 450 nm. Quick decline is because of absorption of light produced by the transition of electrons from the valence band to conduction band of $BiFeO_3$. A high value of transmittance in visible region indicates less deformities and better crystalline nature in ceramics.

According to inter-band absorption theory, the following Tauc relationship can be used for the calculation of optical band gap [38]

$$\alpha h\nu = A\left(h\nu - E_g\right)^n \tag{4}$$

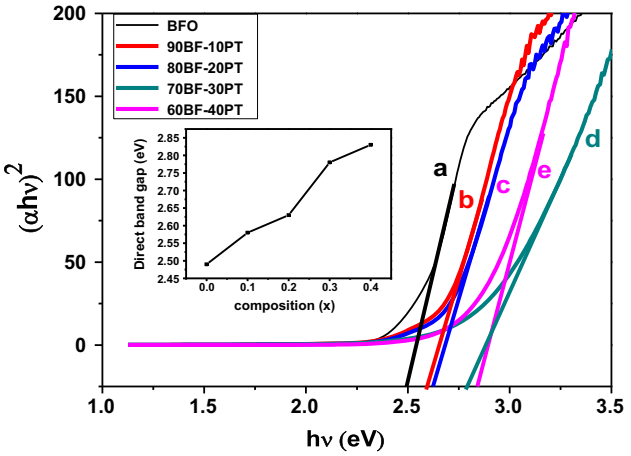


**Fig. 10** Direct energy band gap calculation of the $(BiFeO_3)_{1-x}(PbTiO_3)_x$ solid solutions (a) $x = 0$, (b) $x = 0.1$, (c) $x = 0.2$, (d) $x = 0.3$ and (e) $x = 0.4$

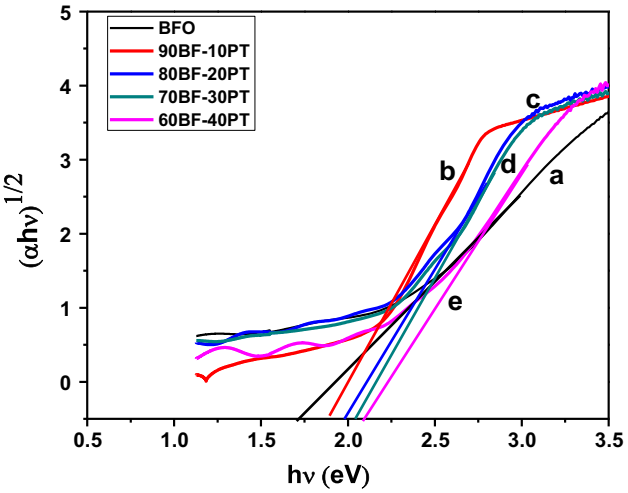


**Fig. 11** Indirect energy band gap calculation of the $(BiFeO_3)_{1-x}(PbTiO_3)_x$ solid solutions (a) $x = 0$, (b) $x = 0.1$, (c) $x = 0.2$, (d) $x = 0.3$ and (e) $x = 0.4$

where $A$ represents probability parameter, which is independent of photon energy $h\nu$ and energy band gap $E_g$, α is the absorption coefficient and n is index indicating the transition type (1/2 for direct transition and 2 for indirect transition). In different studies, energy band gap of $BiFeO_3$ at normal temperature is mentioned from 2.3 to 2.8 eV [39–43]. As reported by some researchers, this band gap is direct, [41,42], whereas different reports additionally recommended the appearance of indirect band gap smaller than the direct band gap [39,40]. Maximum energy state in valence is situated at the R-point corner of the Brillouin zone, though the minimum energy state in conduction band is at the middle, Γ, indicating the indirect band gap of BFO [44]. However, the calculated valence band in the rhombohedral structured BFO is nearly flat [43]; therefore, $BiFeO_3$ ought to be performed as a direct band gap semiconductor at room temperature.

Figure 10 shows plotting of $(\alpha h\nu)^2$ versus $h\nu$ for $BiFeO_3$ and BF–PT composite. A linear variation of $(\alpha h\nu)^2$ in a certain range favors the supposition of a direct energy band gap. Sharp rise of absorbance close to the absorption edge indicates transition of direct type. So, direct energy band gap of $BiFeO_3$ and BF–PT composite was figured out by extrapolating the linear part of the curves $(\alpha h\nu)^{\frac{1}{n}} = 0$ (Fig. 10). Some research papers reported appearance of indirect band gap of $BiFeO_3$, so we also calculated indirect band gap of BF–PT system by extrapolating straight region of $(\alpha h\nu)^{\frac{1}{2}}$ versus photon energy $(h\nu)$ as plotted in Fig. 11. Linear variation in high energy domain of plots $(\alpha h\nu)^2$ and $(\alpha h\nu)^{\frac{1}{2}}$ indicates that both direct and indirect transitions are present in $BiFeO_3$ and BF–PT composite. Estimated direct and indirect band gaps for BFO and various samples of BF–PT are given in Table 2. The estimated direct energy band gap $(E_g)$ of BF–PT composite is higher than direct band gap of $BiFeO_3$ (2.49 eV). The value of $E_g$ for bulk $BiFeO_3$ is nearly same as that of $BiFeO_3$ (2.50 eV) determined by applying the first principles within generalized gradient approximation [45], while it is smaller than the value of direct gap (2.74 eV) obtained by multiple-angle spectroscopic [40]. Variation of the band gap of $(BiFeO_3)_{1-x}(PbTiO_3)_x$ with composition '$x$' is shown in the inset of figure 10. The energy band gap of bulk $PbTiO_3$ (3.19 eV) is greater than energy band gap of BFO (2.49 eV). Accordingly, addition of content of $PbTiO_3$ should increase the band gap energy of $(BiFeO_3)_{1-x}(PbTiO_3)_x$. Therefore, the direct energy band of all composition of $(BiFeO_3)_{1-x}(PbTiO_3)_x$ is greater than recognized band gap (2.49 eV) of $BiFeO_3$ [46].

## 4 Conclusions

Basic structural examination has exhibited the presence of morphotropic phase boundary in $(BiFeO_3)_{1-x}(PbTiO_3)_x$ ceramics with perovskite phases of rhombohedral and tetragonal symmetry existing simultaneously. Chemical homogeneity of BF–PT samples by EDAX was found to be in good agreement with their actual composition. Weak ferromagnetism at the temperature of 5 K was observed in BF–PT system by the substitution effect of $PbTiO_3$. Linear behavior of M-H plot for BFO sample indicated the antiferromagnetic nature of BFO. Low-temperature (5–300 K) magnetization of $(BiFeO_3)_{1-x}(PbTiO_3)_x$ ceramics samples under zero-field cooling (ZFC) condition exhibited an anomaly in tetragonal phase of MPB for composition $x = 0.2$ and 0.3. Antiferromagnetic transition temperature $(T_{N-t})$ corresponding to tetragonal phase for $x = 0.2$ and 0.3 was measured as 252 K and 243 K, respectively. Incorporation of $PbTiO_3$ indicated the enhancement of ferroelectricity

of $(BiFeO_3)_{1-x}(PbTiO_3)_x$ composite. Band gap energy of all compositions of $(BiFeO_3)_{1-x}(PbTiO_3)_x$ appeared to be larger than band gap (2.49 eV) of $BiFeO_3$.

## References


1. Eerenstein, W.; Mathur, N.D.; Scott, J.F.: Multiferroic and magnetoelectric materials. Nature **442**, 759–765 (2006)
2. Cheong, S.W.; Mostovoy, M.: Multiferroics: a magnetic twist for ferroelectricity. Nat. Mater. **6**, 13–20 (2007)
3. Remesh, R.; Spaldin, N.A.: Multiferroics: progress and prospects in thin films. Nat. Mater. **6**, 20–28 (2007)
4. Shariq, M.; Kaur, D.; Chandel, V.C.: Structural, magnetic and optical properties of mulitiferroic $(BiFeO_3)_{1-x}(BaTiO_3)_x$ solid solutions. Chin. J. Phys. **55**, 2192–2198 (2017)
5. Panda, N.; Pattanayak, S.; Choudhary, R.N.P.: Structural and electrical properties of $BiFeO_3-PbTiO_3$ system. J. Mater. Sci. Mater. Electron. **26**, 4069–4077 (2015)
6. Yun, K.Y.; Noda, M.; Okuyama, M.: Prominent ferroelectricity of $BiFeO_3-BiFeO_3$ thin films prepared by pulsed-laser deposition. Appl. Phys. Lett. **83**, 3981–3984 (2003)
7. Comyn, T.P.; Stevenson, T.; Bell, A.J.: Piezoelectric properties of BiFeO–PbTiO ceramics. J. Phys. IV Fr. **128**, 13–17 (2005)
8. Yun, K.Y.; Ricinschi, D.; Kanashima, T.; Noda, M.; Okuyama, M.: Giant ferroelectric polarization beyond $150\,\mu C/cm^2$ in $BiFeO_3$ thin film. Jpn. J. Appl. Phys. **2**(43), L647–648 (2004)
9. Li, J.; Wang, J.; Wutting, M.; Ramesh, R.; Wang, N.; Ruette, B.; Pyatakov, A.P.; Zvedin, A.K.; Viehland, D.: Dramatically enhanced polarization in (001)(001), (101)(101), and (111) (111) $BiFeO_3-BiFeO_3$ thin films due to epitiaxial-induced transitions. Appl. Phys. Lett. **84**, 5261–5263 (2004)
10. Zhang, S.T.; Lu, M.S.; Wu, D.; Chen, Y.F.; Ming, N.B.: Larger polarization and weak ferromagnetism in quenched ceramics with a distorted rhombohedral crystal structure. Appl. Phys. Lett. **87**, 262907–3 (2005)
11. Shariq, M.; Kaur, D.; Chandel, V.C.; Siddiqui, M.A.: Electrical, surface morphology and magneto-capacitance properties of Pb free multiferroic $(BiFeO_3)_{1-x}(BaTiO_3)_x$ solid solutions. Acta Phys. Polon. A **127**, 1679–1679 (2015)
12. Shariq, M.; Kaur, D.; Chandel, V.C.; Siddiqui, M.A.: Investigation on multiferroic properties of $BiFeO_3$ ceramics. Mater. Sci. Pol. **31**, 471–475 (2013)
13. Sosnowska, I.; Loewenhaupt, M.; David, W.I.F.; Ibberson, R.: Investigation of the unusual magnetic spiral arrangement in $BiFeO_3$. Phys. B **117**, 180–181 (1982)
14. Wang, J.; Neaton, J.B.; Zheng, H.; Nagarajan, V.; Ogale, S.B.; Liu, B.; Viehland, D.; Vaithyanathan, V.; Schlom, D.G.; Waghmare, V.U.; Spaldin, N.A.; Rabe, K.M.; Wuttig, M.; Ramesh, R.: Epitaxial $BiFeO_3$ multiferroic thin film heterostructures. Science **299**, 1719–1722 (2003)
15. Dai, X.H.; Xu, Z.; Viehland, D.: The spontaneous relaxor to normal ferroelectric transformation in La-modified lead zirconate titanate. Philos. Mag. B **70**, 33–48 (1994)
16. Kleemann, W.: Random-field induced antiferromagnetic, ferroelectric and structural domain states. Int. J. Mod. Phys. B **7**, 2469–2507 (1993)
17. Wang, Y.P.; Zhou, L.; Zhang, M.F.; Chen, X.Y.; Liu, J.M.; Liu, Z.G.: Room-temperature saturated ferroelectric polarization in $BiFeO_3BiFeO_3$ ceramics synthesized by rapid liquid phase sintering. Appl. Phys. Lett. **84**, 1731–1733 (2004)
18. Behera, C.; Choudhary, R.N.P.; Das, P.R.: Structural and electrical properties of La-modified $BiFeO_3-BaTiO_3$ composites. J. Mater. Sci. Mater. Electron. **25**, 2086–2095 (2014)
19. Wu, Y.J.; Chen, X.K.; Zhang, J.; Chen, X.J.: Magnetic enhancement across a ferroelectric-antiferroelectric phase boundary in $Bi_{1-x}Nd_xFeO_3$. J. Appl. Phys. **111**, 053927-5 (2012)
20. Kawae, T.; Terauchi, Y.; Tsuda, H.; Kumeda, M.: Improved leakage and ferroelectric properties of Mn and Ti codoped thin films. Appl. Phys. Lett. **94**, 112904–3 (2009)
21. Wu, M.S.; Huang, Z.B.; Han, C.X.; Yuan, S.L.; Lu, C.L.; Xia, S.C.: Enhanced multiferroic properties of $BiFeO_3$ ceramics by Ba and high-valence Nb co-doping. Solid State Commun. **152**, 2142–2146 (2012)
22. Sakamoto, W.H.; Yamazaki, W.H.; Iwata, A.; Shimura, T.; Yogo, T.: Synthesis and characterization of $BiFeO_3-PbTiO_3$ thin films through metalorganic precursor solution. Jpn. J. Appl. Phys. **45**, 7315–7320 (2006)
23. Pradhan, S.K.; Das, S.N.; Bhuyan, S.; Behera, C.; Padhee, R.; Choudhary, R.N.P.: Structural, dielectric and impedance characteristics of lanthanum-modified $BiFeO_3-PbTiO_3$ electronic system. Appl. Phys. A **122**, 604–9 (2016)
24. Pradhan, S.K.; Das, S.N.; Bhuyan, S.; Behera, C.; Choudhary, R.N.P.: Structural and electrical properties of lead reduced lanthanum modified $BiFeO_3-PbTiO_3$ solid solution. J. Mater. Sci. Mater. Electron. **28**, 1186–1198 (2017)
25. Burnett, T.L.; Comyn, T.P.; Bell, A.J.: Flux growth of $BiFeO_3-PbTiO_3$ single crystals. J. Cryst. Growth **258**, 156–161 (2005)
26. PCPDFWIN: International Centre for Diffraction Data, 12 Campus Blvd., Newtown Square PA 19073-3273 U.S.A
27. Naheda, B.; Cox, D.E.; Shirane, G.; Gonzala, J.A.; Cross, L.E.; Park, S.E.: A monoclinic ferroelectric phase in the $Pb(Zr_{1-x}Ti_x)O_3$ solid solution. Appl. Phys. Lett. **74**, 2059–2061 (1999)
28. Guo, R.; Crosss, L.E.; Park, S.E.; Noheda, B.; Cox, D.E.; Shirane, G.: Origin of the high piezoelectric response in $PbZr_{1-x}Ti_xO_3$. Phys. Rev. Lett. **84**, 5423–5426 (2000)
29. Catalan, G.; Scott, J.F.: Physics and applications of bismuth ferrite. Adv. Mater. **21**, 2463–2485 (2009)
30. Kumar, M.M.; Srinath, S.; Kumar, G.S.; Suryanarayana, S.V.: Spontaneous magnetic moment in $BiFeO_3-BaTiO_3$ solid solutions at low temperatures. J. Magn. Magn. Mater. **188**, 203–212 (1998)
31. Gehring, G.A.: On the microscopic theory of the magnetoelectric effect. Ferroelectrics **61**, 275–285 (1994)
32. Chen, D.H.; Chen, Y.Y.: Synthesis of barium ferrite ultrafine particles by coprecipitation in the presence of polyacrylic acid. J. Colloid Interface Sci. **235**, 9–14 (2001)
33. Smolenskiĭ, G.A.; Chupis, I.E.: Ferroelectromagnets. Sov. Phys. Uspekhi **25**, 475–493 (1982)
34. Zhu, W.M.; Guo, H.Y.; Ye, Z.G.: Structural and magnetic characterization of multiferroic $(BiFeO_3)_{1-x}$ $(PbTiO_3)_x$ solid solutions. Phys. Rev. B **78**, 014401–10 (2008)
35. Zhu, W.M.; Guo, H.Y.; Ye, Z.G.: Structure and properties of multiferroic $(1-x)BiFeO_3$ $xPbTiO_3$ single crystals. J. Mater. Res. **22**, 2136–2143 (2007)
36. Das, S.R.; Choudhary, R.N.P.; Bhattacharya Katiyara, P.R.S.; Dutta, P.; Manivannan, A.; Seehra, M.S.: Structural and multiferroic properties of La-modified ceramics. J. Appl. Phys. **101**, 034104–7 (2007)
37. Sakamoto, W.; Iwata, A.; Yogo, T.: Ferroelectric properties of chemically synthesized perovskite thin films. J. Appl. Phys. **104**, 104106–8 (2008)
38. Tauc, J. (ed.): Amorphous and Liquid Semiconductor. Plenium Press, New York (1974)
39. Gujar, T.P.; Shinde, V.R.; Lokhande, C.D.: Nanocrystalline and highly resistive bismuth ferric oxide thin films by a simple chemical method. Mater. Chem. Phys. **103**, 142–146 (2007)
40. Fruth, V.; Tenea, E.; Gartner, M.; Anastasescu, M.; Berger, D.; Ramer, R.; Zaharescu, M.: Preparation of $BiFeO_3$ films by wet

chemical method and their characterization. J. Eur. Ceram. Soc. **27**, 937–940 (2007)
41. Ihlefeld, J.F.; Podraza, N.J.; Liu, Z.K.; RaiR, C.; Xu, X.; Heeg, T.; Chen, Y.B.; Li, J.; Collins, R.W.; Musfeldt, J.L.; Pan, X.Q.; Schubert, J.; Ramesh, R.; Schlom, D.G.: Optical band gap of grown by molecular-beam epitaxy. Appl. Phys. Lett. **92**, 142908–3 (2008)
42. Xu, Y.; Shen, M.: Structure and optical properties of nanocrystalline $BiFeO_3$ films prepared by chemical solution deposition. Mater. Lett. **62**, 3600–3602 (2008)
43. Clark, S.J.; Robertson, J.: Band gap and Schottky barrier heights of multiferroic $BiFeO_3$. Appl. Phys. Lett. **90**, 132903–3 (2007)
44. Catalan, G.; Scott, J.F.: Physics and applications of bismuth ferrite. Adv. Mater. **21**, 2463–2485 (2009)
45. Liu, K.; Fan, H.; Ren, P.; Yang, C.: Structural, electronic and optical properties of BiFeO3 studied by first-principles. J. Alloys Compd. **509**, 1901–1905 (2011)
46. Chena, Y.; Zhoua, X.; Zhaoa, X.; Hea, X.; Gub, X.: Crystallite structure, surface morphology and optical properties of $In_2O_3-TiO_2$ composite thin films by sol-gel method. Mater. Sci. Eng. B **151**, 179–186 (2008)